JOURNAL OF MATERIALS SCIENCE 28 (1993) 3675–3680

Film-thickness effects on the optical and electrical properties of Cu–GeO_2 thin cermet films

A. M. AL-SAIE, M. H. RAHMAN
Department of Physics, University of Bahrain, PO Box 32038, Bahrain
J. BEYNON
Department of Physics, Brunel University, Uxbridge, Middlesex, UB8 3PH, UK

The effect of film thickness on the optical and electrical properties of Cu–30 wt% GeO_2–70 wt% thin cermet films prepared by electron-beam deposition at about 10^{-3} Pa and at a substrate temperature of 300 K is reported. The ultraviolet, visible and direct current (d.c.) conductivity results are analysed with the aim of determining the optical band gap, E_{opt}, the width of the band tails, E_e, and the d.c. thermal activation energy, E_a. It was found that the optical energy gap increases with increasing thickness and that the absorption was due to indirect transitions in k-space. The general feature of the absorption edge remains similar for both unannealed and annealed films, but annealing has the effect of decreasing E_{opt}. The d.c. conductivity results show that E_a decreases with increasing thickness. From a knowledge of E_{opt} and E_a, a probable model of the electronic band structure in Cu–GeO_2 thin films has been suggested.

1. Introduction

Extensive studies of ceramic–metal (cermet) thin films have been carried out for many years because of their potential applications in integrated circuits [1–11]. The excellent transmittance (about 92%) of the cermets in the visible region and continuous variation of the absorption coefficient as a function of photon energy make them ideal as photoelectric devices, absorption filters and other optical elements [12]. These films are primarily insulators with metal incorporated. Optical and electrical characterizations were studied of cermet films with various metal and dielectric compositions, such as Mn–SiO [3], Cu–SiO_x [5] and Au–SiO_2 [6], which were prepared by various deposition techniques.

Some thickness-dependent optical and electrical properties of Cu–GeO_2 films were investigated. The main purpose was to examine optical absorption and d.c. conductivity, in terms of the models currently in use, and to describe these properties. Determinations of the optical band gap, E_{opt}, the refractive index n, the width E_e of the tail of localized states in the band gap and the d.c. thermal activation energy, E_a, are often necessary to develop the electronic band structures of amorphous materials [3]. The theoretical work of Davis and Mott [7] and Tauc *et al.* [8] have generally established that for many amorphous materials in the higher absorption region ($\alpha > 10^4\ cm^{-1}$) the absorption coefficient $\alpha(\nu)$ is described by

$$\alpha(\nu) = B(h\nu - E_{opt})^2/h\nu \quad (1)$$

where ν is the photon frequency, h is Planck's constant and B is a constant. Furthermore, for many amorphous materials, the low-frequency end of the band gap shows an almost linear relation on a logarithmic scale. This behaviour has often been referred to in the literature as the Urbach behaviour [9]. For $\alpha(\nu) < 10^4\ cm^{-1}$, this may be expressed by the relation

$$\alpha(\nu) = \alpha_0 \exp(\hbar\omega/E_e) \quad (2)$$

where α_0 is a constant.

The dielectric function, ε, is a fundamental property of the cermets, and it can be used to calculate the optical gap. To determine this parameter it is essential to know K, the extinction coefficient. Further, much of the optical behaviour of the films can be understood when n and K are plotted as a function of the incident photon energy. Once $\alpha(\nu)$ is known, the parameter K can be calculated according to the relation,

$$K = \frac{\alpha(\lambda)\lambda}{4\pi} \quad (3)$$

D.c. conductivity was measured with the aim of determining the activation energy. Various theories have been proposed to account for the electrical conduction mechanism in thin films [7, 10, 11, 13–15]. Depending on the size and spacing of the conducting particles in a dielectric matrix, as well as the temperature variation, conduction may occur via quantum-mechanical tunnelling, thermionic emission or hopping. In the case of semiconducting amorphous materials, the conduction mechanism can be attributed to any one of, or a combination of, the above

0022–2461

three processes. In our present study we find that all cermets are well described by

$$\sigma = \sigma_0 \exp(-E_a/kT) \quad (4)$$

in the high temperature region ($T > 323$ K). Here σ_0 is a constant. Equation 4 indicates that conduction may be due to thermionic carrier excitation from extended states of the valance band to those of the conduction band.

2. Experimental techniques

2.1. Preparation of the films

Thin films of varying thickness (227–407 nm) were prepared by electron-beam evaporation of appropriate mixes of Cu and GeO_2 powder (pressed in the shape of pellets) from a single graphite boat at a pressure of about 10^{-3} Pa and a substrate temperature of 300 K. Corning 7059 glass substrates were ultrasonically cleaned in a series of conventional steps and by a glow-discharge cleaning process. The substrates were positioned centrally, relative to the source, and the films were deposited on to them at a beam voltage of 3 kV and a beam current of 10–12 mA, corresponding to deposition rates within 2–3.5 nm s^{-1}. The deposition rate and thickness were controlled by reflection interference of a He–Ne laser beam during the growth of the film using a photosensor, the output of which was then fed to a x–y plotter via a lock-in amplifier. The reflection–transmission curve (Fig. 1) obeyed the following relation [16]

$$t = \frac{\lambda X}{4n} \quad (5)$$

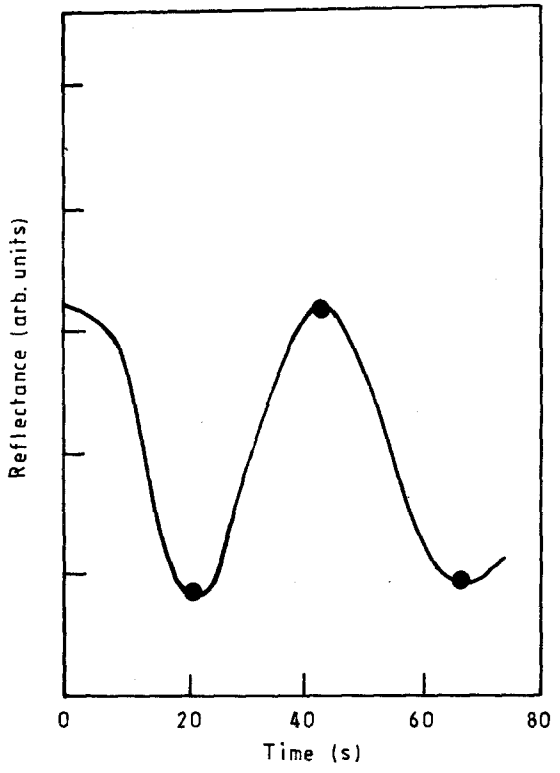

Figure 1 Reflectance (in arbitrary units) as a function of growth time of the film A. Number of reflection and transmission peaks, X, and thickness, t, are according to Equation 5. (A) $X = 3\frac{1}{2}$

where t is the thickness of the film, λ is the laser wavelength, X is the number of reflection and transmission peaks and n is the refractive index of the film.

2.2. Spectroscopic measurements and determination of film thickness, refractive index and absorption coefficient

The optical-transmission measurements in the range 550–2000 nm were carried out using a Cary 2300 double-beam spectrophotometer with automatic data acquisition by computer. Transmission spectra for samples C and D were obtained but no such spectra were obtained for samples A and B, indicating that the latter were too thin to form interference fringes. Fig. 2 shows the transmission spectra for sample C. Using the Swanepoel technique [16] (which is based on creating envelopes of transmission maxima and minima), the refractive index, n, and film thickness, t, were determined according to the following relations:

$$n = [N + (N^2 - S^2)^{1/2}]^{1/2} \quad (6)$$

where

$$N = 2S\frac{(T_M - T_m)}{T_M T_m} + \frac{S^2 + 1}{2}$$

and

$$t = \frac{\lambda_1 \lambda_2}{2(\lambda_1 n_2 - \lambda_2 n_1)} \quad (7)$$

Here n_1 and n_2 are the refractive indexes at two adjacent maxima or minima corresponding to wavelengths λ_1 and λ_2 respectively. T_M and T_m are the values of the transmission maximum and corresponding minimum at specific wavelengths. S is the refractive index of the substrate.

The refractive index of the substrate was found to be constant in the region 500–1000 nm and was calculated from the transmission curve (Fig. 2) according to the relation [16],

$$S = \frac{1}{T_s} + \left(\frac{1}{T_s^2 - 1}\right)^{1/2} \quad (8)$$

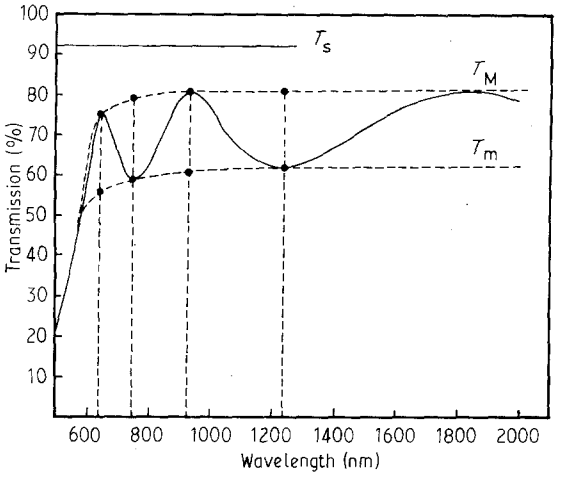

Figure 2 Transmission spectra for a 407 nm thick film of Cu–GeO_2 on Corning-7059-glass substrate with transmission T_s. Curves T_M and T_m according to the text.

TABLE I Optical properties of Cu–30 % GeO_2–70 % cermet films deposited at a substrate temperature of 300 K and at a vacuum pressure of 10^{-3} Pa

Films	Thickness (nm)	Deposition rate R ($nm\,s^{-1}$)	Before annealing		After annealing	
			E_{opt}(eV)	E_e(eV)	E_{opt}(eV)	E_a(eV)
A	227	3.2	1.69	0.60	1.30	1.08
B	340	2.0	1.96	1.23	1.70	1.01
C	407	3.1	1.99	0.64	1.85	0.68
D (GeO_2)	395	3.5	2.80	–	2.86	1.17

The transmittance T_s of the substrate was found to be 0.93 from which S was calculated to be 1.51. The thickness of sample C was found to be 407 nm and of sample B 340 nm. These values enabled the refractive index to be calculated, in the range 2.31–2.39, as a function of wavelength. The Swanepoel method has been used by many authors for amorphous thin films and has been found to be accurate to $\pm$ 1% [17, 18].

The refractive index of sample A, corresponding to a He–Ne laser wavelength of 632.8 nm, was determined from the transmission curve of C. Using Equation 5 with the values of X from Fig. 1, the thickness of sample A was calculated. The same technique was used to calculate the thickness of sample B. These values are listed in Table I.

The optical absorption measurements in the range 270–800 nm were also carried out using the Cary 2300 spectrophotometer. A Corning glass was used as a reference to eliminate the effect of substrate absorption. The absorption coefficient $\alpha(\nu)$ was obtained using the standard relation

$$\alpha(\nu) = t^{-1} \ln A \qquad (9)$$

where A is the absorbance of the films.

2.3. Annealing and d.c. conductivity measurements

Differential scanning calorimetry (DSC) was performed to ensure that the annealing temperature was lower than the glass transition temperature, T_g. No structural or phase changes were observed up to 500 °C. Therefore, the films were annealed at 250 °C at ambient atmosphere for 2 h and the specimens were then cooled to room temperature at a rate of $2\,°C\,min^{-1}$.

D.c. conductivity was measured in the range 573–323 K using a HP 4140 B PA meter which acted as a voltage source and a picoammeter. A HP 3497A data-acquisition unit was used to measure the potential drop across the thermocouple. All measurements were carried out under the control of a HP 9836 A computer.

3. Results and discussions

3.1. Optical absorption

Figs 3 and 4 show the optical absorption spectra at different thicknesses for unannealed (Fig. 3) and annealed (Fig. 4) Cu–GeO_2 and GeO_2 films. In Fig. 3,

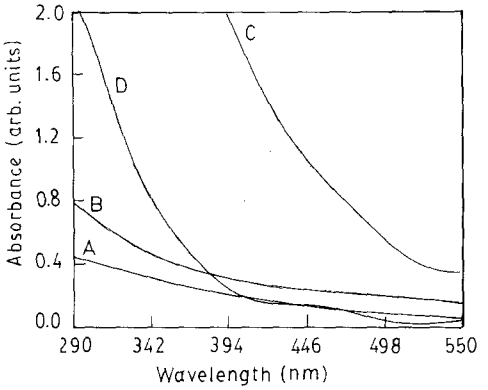

Figure 3 Absorption spectra for annealed films as function of wavelength for film thickness: (A) 227 nm, (B) 340 nm, (C) 407 nm, and (D) 395 nm (GeO_2).

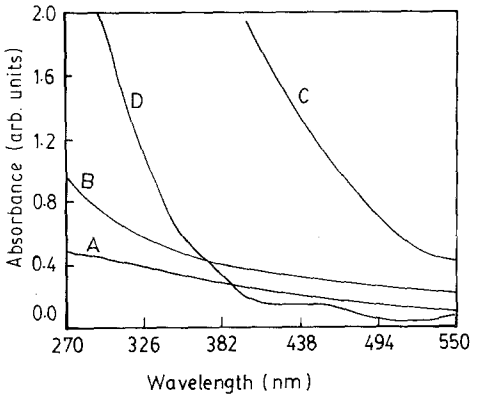

Figure 4 Absorption spectra for annealed films as a function of wavelength for film thicknesses: (A) 227 nm, (B) 340 nm, (C) 407 nm, and (D) 395 nm (GeO_2).

the optical absorption edge, which is defined as the photon energy at which absorption starts increasing from zero, shifts towards higher wavelengths with increasing film thickness. This feature is generally retained for unannealed films in Fig. 4, although the absorption edges are seen to move towards higher wavelengths leading to a decrease in the values of E_{opt}. Figs 5 and 6 show the graphs of $(\alpha h\nu)^{1/2}$ against photon energy for unannealed and annealed films, respectively. The graphs have well defined linear regions which confirm that the cermets and GeO_2 films obey Equation 1. Values of E_{opt} are obtained by extrapolating the linear portions. These values are listed

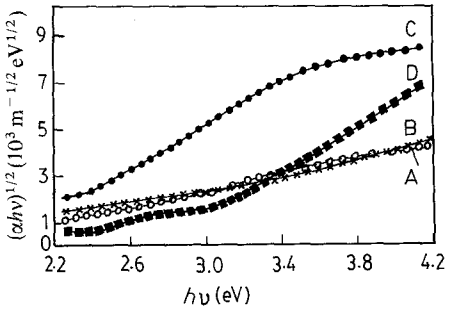

Figure 5 Optical absorption for unannealed films replotted in accordance with Equation 1: (A, B, C) Cu–GeO_2 cermets, and (D) amorphous GeO_2.

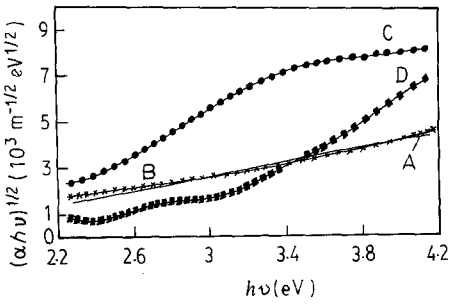

Figure 6 Optical absorption for annealed films replotted in accordance with Equation 1: (A, B, C) Cu–GeO_2 cermets, and (D) amorphous GeO_2.

in Table I. It is seen that E_{opt} systematically decreases as the thickness of the films decreases. Some explanations for the variation of E_{opt} with thickness are given in [13]. The authors of [13] contend that dangling bonds created during the deposition process might introduce some structural defects in the films. In turn, these defects form localized states in the material. As the film thickness grows, these defects and, hence, the localized states are reduced and the films become more homogeneous and amorphous. As a result, E_{opt} increases. E_{opt} for 100% GeO_2 (395 nm) is estimated to be 2.80 eV whereas that for Cu–GeO_2 (sample C, 407 nm) is found to be 1.99 eV. Because these two films have almost equal thickness and have been produced under identical deposition conditions, it appears that the addition of Cu to the matrix of GeO_2 produces a reduction in E_{opt}. Similar observations have been made by other authors [3] for the Mn–SiO system. It may be noted that for 100% SiO, E_{opt} has been reported to be 2.73 eV (852 nm) for slow rates of evaporation [13] whereas for 100% amorphous GeO_2 glass, E_{opt} was reported to be 3.75 eV [19].

As seen from Table I, the values of E_{opt} for annealed cermet films are smaller than those of unannealed films, which is consistent with the shift of the absorption spectra towards higher wavelengths (Fig. 5). This shift may be associated with crystallization of the films during annealing, resulting in a decrease in thickness and an increase in refractive index, leading to more optically dense films. The factor $(\alpha h\nu)^{1/2}$ increases as the film thickness increases, resulting in a higher transition probability of carriers across the optical gap

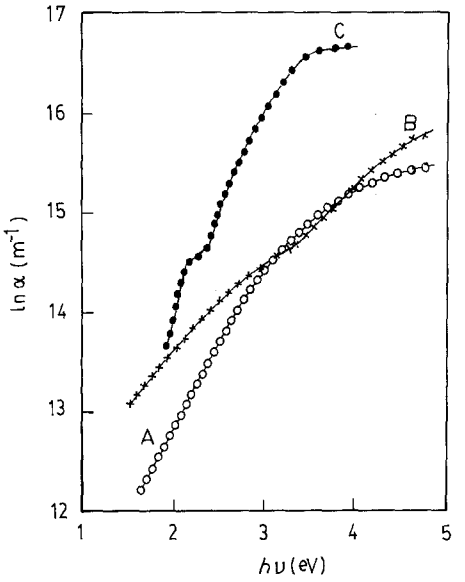

Figure 7 General shape of the absorption edge of the cermets for film thicknesses: (A) 227 nm, (B) 340 nm, and (C) 407 nm.

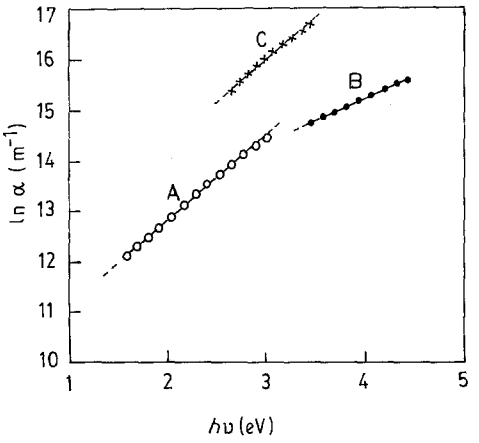

Figure 8 Urbach behaviour of the absorption edge plotted in accordance with Equation 2.

[20]. This may occur as impurity bands redistribute themselves closer to the Fermi level.

3.2. The Urbach behaviour

Fig. 7 represents the general shape of the absorption edge of Cu–GeO_2 cermets. For each film, it is seen that $\alpha(\nu)$ increases exponentially with $h\nu$ in certain regions suggesting that the Urbach rule (Equation 2) is being followed. These regions are shown in separate plots in Fig. 8. The values of the band tail width E_e are calculated from the slopes of these curves and are listed in Table I. The values vary between 0.60 and 1.23 eV. From this, there does not appear to be any systematic dependence of E_e on thickness. These values are quite large compared to those of many amorphous semiconductors [21] but are consistent with those of Mn–SiO cermets [3] (0.45–1.10 eV) depending on Mn concentration and deposition parameters such as rate of evaporation and pressure. Moridi and Hogarth [12] found that E_e lay between 0.66 and 1.06 eV for various

Cu concentrations in copper–calcium phosphate glasses.

Many theoretical and experimental explanations have been put forward for the Urbach behaviour [14, 15, 22–25]. Though Urbach edges have been observed in many crystalline and amorphous materials, no single model is sufficient to explain their origin. Redfield [22] attributes this effect to frequency-dependent fluctuations of microfields caused by impurities. This scenario is closely related to an electron-impurity scattering process that results in lattice distortion and band-tail behaviour in amorphous materials. Tauc [24] proposed that this behaviour is due to electronic transitions between localized states and that the width of the tail, E_e, will vary with composition and deposition parameters. Davis and Mott [7] dispute Tauc's proposal on the ground that Urbach edges occur in many amorphous semiconductors with roughly similar slopes at room temperature. Dow and Redfield [23] sugget that the Urbach edges arise from an electric-field broadening of an exciton in the localized states. Davis and Mott dispute this idea too.

In our present work, the values of E_e vary significantly with thickness and, as indicated earlier, many authors have reported E_e to be significantly dependent on compositions. These observations contradict the Davis–Mott hypothesis and lend support to the Tauc-model in which the Urbach edge arises from electronic transitions between localized states at the band tails.

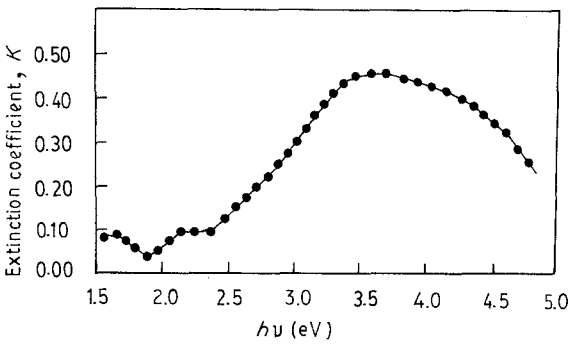

Figure 9 Spectral dependence of the extinction coefficient $K(\lambda)$ on photon energy for the film C (407 nm).

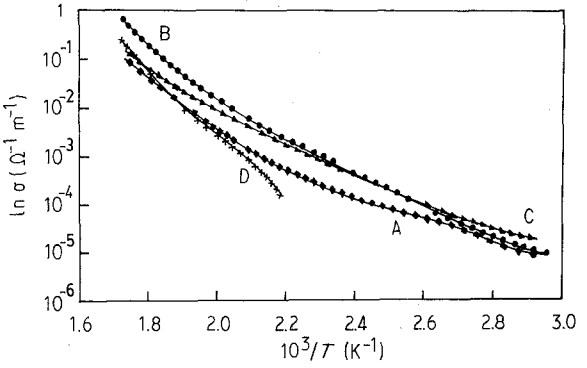

Figure 10 Conductivity plotted in accordance with Equation 4 for the cermets: (A) 227 nm, (B) 340 nm, (C) 407 nm, (D) 395 nm (GeO_2).

3.3. The refractive index $n(\lambda)$ and the extinction coefficient $K(\lambda)$

The complex refractive index of the films is given by

$$\hat{n}(\lambda) = n(\lambda) - iK(\lambda)$$

$n(\lambda)$ for the sample C was calculated from the transmission spectra (Fig. 2) using Equation 6 and was found to vary between 2.31 and 2.39 in the wavelength range 900–600 nm. $K(\lambda)$ was calculated using Equation 3. Fig. 9 illustrates the spectral dependence of $K(\lambda)$ on photon energy for sample C. In this figure three spectral regions can be identified. In the visible region (800–500 nm) K is very small, this is a transparent region with low absorption. At the approach of the band gap (1.99 eV), K increases rapidly; this is a highly absorbing region. At energies greater than 3.5 eV, K decreases and the film tends to become transparent again. Such dispersion of the optical properties is usually attributed to excitation of carriers from the extended states of the valence band to the conduction band.

3.4. D.c. conductivity and energy-band diagram

Fig. 10 shows graphs of ln σ versus T^{-1} in the temperature region 573–323 K. Equation 4 appears to be obeyed by all films. E_a is calculated from the gradients of the linear portions of these curves and is listed in Table I. It is found that with increasing film thickness, E_a decreases systematically. Furthermore, on comparing E_a for sample C with that of the sample D, it may be noted that incorporation of Cu in the matrix of GeO_2 has the effect of decreasing the activation energy. Further, E_a is less than $\frac{1}{2} E_{opt}$. Thus, it may be assumed that an impurity band exists within the mobility gap. For sample C, the impurity band would be located about 0.68 eV below the Fermi level. Assuming that the Fermi level is midway between the valence and conduction bands, a probable model of the electronic band structure in Cu–GeO_2 cermet thin films may be suggested (Fig. 11). As E_{opt} is 1.85 eV, the mobility gap can be calculated to be 2.34 eV.

The variation of E_a with thickness can be explained if it is assumed that E_a is proportional to r^{-1}, where r is the average linear dimension of a Cu particle [10]. In the present investigation, thermally activated conduction is assumed to take place between two Cu particles separated by a space filled with GeO_2. As the film thickness grows, the space between the two Cu particles decreases and the dimensions of the particles increase leading to smaller activation energies. Morris [6] and Miller *et al.* [26] found that the electrostatic charge-activated tunnelling well explained the conduction mechanism in Au–SiO systems. However, it may be noted from Fig. 11 that the potential barrier is 2.34 eV, which is much smaller than that found for Au–SiO (3.7 eV) by Miller *et al.* [26]. Steele and Beynon [27] report thermally activated polaron hopping between localized tail states as the dominant mode of conduction for Au–SiO_x films with a metallic content of 16 wt %. However, the conduction mechanism in Cu–GeO_2 films cannot be determined unless

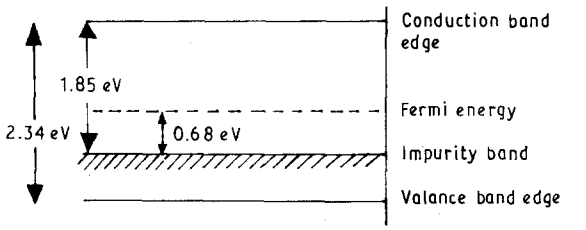

Figure 11 A tentative energy band diagram for the cermet Cu–GeO_2 (407 nm).

thermoelectric and Hall-effect measurements are made on the same samples. These aspects of the conduction mechanism will be the subject of further studies by us.

4. Conclusion

Spectroscopic measurements show that

1. The optical energy gap increases with increasing thickness and absorption is due to indirect transitions in k-space.

2. Incorporation of Cu in the matrix of GeO_2 introduces defect states leading to a reduction in E_{opt}.

3. Annealing has the effect of decreasing E_{opt}.

D.c. conductivity measurements indicate that:

1. Thermal activation energy decreases with increasing thickness.

2. In high temperature regions, conductivity is described well by Equation 4.

Acknowledgements

We express our gratitude to Dr K. Mirza of the Physics Department, University of Bahrain for helping us with the computational analysis. We are also thankful to Professor C. A. Hogarth of Brunel University for many useful discussions.

References

1. J. E. MORRIS and T. J. COUTTS, *Thin Solid Films* **47** (1977) 1.
2. Z. H. MEIKSIN, *Phys. Thin Film* **8** (1975) 99.
3. S. K. J. AL-ANI, M. A. R. SARKAR, J. BEYNON and C. A. HOGARTH, *J. Mater. Sci.* **20** (1985) 1637.
4. R. DAHAN, J. PELLEG and L. ZEBIN, *J. Appl. Phys.* **6** (1990) 67.
5. J. LI and J. BEYNON, *Phys. Status Solidi* (a) **128** (1991) 151.
6. J. E. MORRIS, *Thin Solid Films* **11** (1972) 299.
7. E. A. DAVIS and N. F. MOTT, *Phil. Mag.* **22** (1970) 903.
8. J. TAUC, R. GRIGORVICI and A. VANCU, *Phys. Status. Solidi.* **15** (1966) 627.
9. F. URBACH, *Phys. Rev.* **92** (1953) 1324.
10. C. A. NEUGEBAUER and M. B. WEBB, *J. Appl. Phys.* (1) **33** (1962) 74.
11. R. M. HILL and T. J. COUTTS, *Thin Solid Films* **42** (1977) 201.
12. G. R. MORIDI and C. A. HOGARTH, in Proceedings of the 7th International Conference on Amorphous and Liquid Semiconductors, Edinburgh, June 1977, edited by W. E. Spear, University of Edinburg (Centre for Industrial Consultancy and Liason, Edinburgh 1977) p. 688.
13. S. K. J. AL-ANI, K. I. ARSHAK and C. A. HOGARTH, *J. Mater. Sci.* **19** (1984) 1737.
14. M. V. KURIK, *Phys. Status Solidi* (a) **8** (1970) 9.
15. D. J. DUNSTAN, *J. Phys. C* **30** (1982) L419.
16. R. SWAWNEPOEL, *J. Phys. E* **96** (1983) 1214.
17. E. MARQUEZ, J. RAMIREZ-MALO, P. VILLARES, R. JIMENEZ-GARAY, P. J. S. EWEN and A. E. OWEN, *J. Phys. D* **25** (1992) 535.
18. M. HAMMAM, M. A. HARTH and W. H. OSMAN, *Solid State Commun.* **59** (1986) 271.
19. M. N. KHAN and E. E. KHAWJA, *Phys. Status. Solidi.* (a) **74** (1982) 273.
20. S. CHOUDHURY, S. K. BISWAS, A. CHOUDHURY and K. GOSWAMI, *J. Non. Cryst. Solids* **46** (1981) 171.
21. N. F. MOTT and E. A. DAVIS, in "Electronic processes in non-crystalline materials" 2nd Edition (Clarendon Press, Oxford, 1979).
22. D. REDFIELD, *Phys. Rev.* **130** (1963) 916.
23. J. D. DOW and D. REDFIELD, *Phys. Rev.* **B5** (1972) 594.
24. J. TAUC, in "The optical properties of solids", edited by F. Abeles (North Holland, Amsterdam, 1970) p. 277.
25. T. SKETTRUP, *Phys. Rev. B* **18** (1978) 2622.
26. N. C. MILLER, B. HARDIMAN and G. A. SHIRN, *J. Appl. Phys.* (4) **41** (1970) 1850.
27. C. B. STEELE and J. BEYNON, *Phys. Status Solidi* (a) **106** (1988) 515.

Received 17 August
and accepted 14 September 1992